Nanoscale Distribution of Ryanodine Receptors and Caveolin-3 in Mouse Ventricular Myocytes: Dilation of T-Tubules near Junctions

Joseph Wong,[†△] David Baddeley,[‡△] Eric A. Bushong,[†] Zeyun Yu,[§] Mark H. Ellisman,[†] Masahiko Hoshijima,[†¶]* and Christian Soeller*

[†]Center for Research in Biological Systems and [¶]Department of Medicine, University of California San Diego, La Jolla, California; [‡]Department of Physiology, School of Medical Sciences, University of Auckland, New Zealand; and [§]Department of Computer Science, University of Wisconsin-Milwaukee, Milwaukee, Wisconsin

Received for publication 3 December 2012 and in final form 25 February 2013.

*Correspondence: c.soeller@auckland.ac.nz or mhoshijima@ucsd.edu

Editor: Leslie Loew.

[△]Joseph Wong and David Baddeley equally contributed to this work.

David Baddeley's present address is Department of Cell Biology, Yale University, New Haven, Connecticut

Christian Soeller's present address is Biomedical Physics, University of Exeter, United Kingdom

Supplementary Material: Methods

Immuno-fluorescent staining

Animal procedures in the current study were approved by the University of California San Diego Institutional Animal Care and Use Committee. Adult mouse ventricular cardiomyocytes were isolated from 4-5 month-old C57BL/6 male mice by collagenase perfusion-digestion, as described previously (1) and the cells were immediately fixed in 2% paraformaldehyde for 10 min after isolation. Immuno-fluorescent staining was carried out as described previously (2) (3). A mouse-anti-RyR2 primary antibody (Ab, 1:100, Thermo Scientific, MA3-916) and a rabbit polyclonal anti-Cav3 Ab (1:500, Abcam, AB2912) were used followed by the incubation with highly-cross adsorbed Alexa 680-labeled goat anti-mouse IgG and Alexa 750-labelled goat anti-rabbit IgG antibodies (1:100, Invitrogen). Finally the cells were transferred into a "mounting medium" containing 90% (v/v) Glycerol (v/v), 10% (v/v) PBS (v/v), 10% (w/v) glucose, 10 mM cysteamine, 0.5 mg/mL glucose oxidase, and 50ug/mL catalase. The suspended cells were mounted on a clean coverslip (thickness #1.5) and sealed to a slide grass using nail varnish.

Setup and acquisition for 2D and 3D dSTORM imaging

The imaging system used in the current study has been described (3, 4). In brief, it consists of a Nikon TE2000 inverted microscope with a custom objective holder, a piezo focuser (P-725, Physik Intrumente, Germany), an EMCCD camera (DV887, Andor Technology, UK), a custom image splitting device which allows for the simultaneous detection of multiple color channels, custom illumination optics, and a number of laser sources. For 2-dimensional imaging, samples were imaged either near the cell surface or approximately 5 μm from the cell surface. Fluorescence was excited using a single 671 nm diode laser (Viasho, China), which was coupled into the microscope so as to produce a highly inclined light sheet (5) within the sample. Data was recorded simultaneously from both Alexa 680 and Alexa 750 labeled structures and single molecule events fitted in both long and short channels simultaneously with color assignment being performed on the basis of the ratio of the intensities as described previously(4) . A series of ~20,000 raw frames (50 ms/frame) were captured for each reconstruction. For 3D localization a 500 mm focal length astigmatic lens was inserted into the optical path in a collimated light region within the splitter device resulting in a focus separation of ~400 nm. For 3D localisation, PSFs were measured and fitting was performed as described (4).

Co-localization analysis

Images were rendered from the event position data using an algorithm based on a jittered Delaunay triangularization, as described previously (6). The resulting images are linear in event density and thus effectively equivalent to conventional fluorescence images in which the density of marker molecules determines the local intensity albeit exhibiting substantially higher resolution.

These images were then thresholded using the isodata algorithm to obtain binary masks of the RyR or Cav3 distribution. Co-localization was quantified on the basis of these masks using Manders coefficients (7). In addition to the Manders co-localization figure, which is typically very low in super-resolution images, we performed a distance transform based analysis, in which the amount of labeling in one channel at a given distance from the edge of the other channel's mask was calculated, as described (3). By calculating the amount of labeling at a given distance from the edge of the masks, using the convention that distances within the cluster mask were negative whereas distances outside the mask were positive, fractions of total labeling as a function of distance were determined. The fractions were summarized in distance histograms (as shown in Figs 1 & 2). The approach is similar to the analysis described in (8) .

The resulting distance histograms were normalized (as shown in Fig 1). In super-resolution data, numerical co-localization values are typically very low and the portrayal as a distance histogram allows an analysis of association at distances larger than the resolution limit, such as typical Ca^{2+} diffusion distances, by summing the bins less or equal to the distance of interest.

Analysis of T-system diameters

T system diameters were estimated using custom-written IDL routines that analyzed t-system segments. The segments were selected by tracing centerlines of t-tubule segments (typically ~2 μm long) within rendered super-resolution images using the segmented-line ROI tool in ImageJ (Figure 2D). The images and ROIs were then exported to IDL and IDL subroutines extracted straightened intensity distributions along the ROI lines of both CAV3 and RyR signal as seen in Fig. 2E. From these intensity distributions full-width at quarter of maximum (FWQM) masks were calculated at every point along the t-tubule segment (see Fig. 2F) and used to determine local diameters. We used FWQM (as opposed to half-maximal values) to reduce the sensitivity to signal variations across tubules. To illustrate the typical difference between these measures we compared full-width at half maximum (FWHM) diameters in a single cell and obtained in regions distant to dyads ~85 nm FWHM versus ~130 nm FWQM. The FWQM t-tubule diameters were classified according to the presence or absence of RyR signal into three groups: ex-dyad, dyad(CAV3) and dyad(CAV3 & RyR). "Ex-dyad" regions were defined to be sections of the t-tubule where there was no overlap between RyR and CAV3 signals (Figure 2D) while overlapping RyR and CAV3 were used to identify the dyad regions. Dyad region diameters were measured in two ways: (a) using only CAV3 channel masks (termed "dyad(CAV3)") and (b) using both CAV3 and RyR channel masks (termed "dyad(CAV3 & RyR)"). A qualitative comparison of EM tomogram data and super-resolution images suggested that the combined CAV3 and RyR masks provide a more faithful estimate of the extent of t-system lumen in the vicinity of junctions, see Fig. S3.

Statistical testing

The diameter data was tested for statistical differences by comparing the pooled histogram data using a Kolmogorov-Smirnov test and ex-dyad diameters were different from both dyad(CAV3) and dyad(CAV3&RyR) diameters, $p<0.01$. In addition, mean diameters were calculated for all 3 classes on a

per cell basis (n=6 cells) and mean ex-dyad diameters were different from both dyad(CAV3) and dyad(CAV3&RyR) diameters on the basis of a Wilcoxon rank test, $p<0.01$, see also Fig. 2H.

Electron microscopy

EM tomograms of ventricular cardiomyocytes were prepared from 3-6 months old 129/Sv mice as described previously (9). Briefly, sections cut at 500 nm thickness were imaged at 15,000× magnification and angular increments of 2° from −60° to +60° using a JEOL 4000EX intermediate voltage electron microscope operated at 400kV. Tomograms were reconstructed using a transform-based back projection algorithm, TxBR (10). Geometric features of membrane organelles were segmented in IMOD (Boulder Laboratory for 3-D Electron Microscopy of Cells, University of Colorado, Boulder, CO) (11) and triangular surface meshes were generated for visualization in IMOD or in Amira (Mercury Computer Systems Inc., Boston, MA).

For block face scanning EM (SBFSEM) imaging, 4-month old C57BL/6 male mice were perfusion-fixed as described previously (9). Tissues were sectioned using a vibratome (Leica VT1000S) in 0.15 M sodium cacodylate buffer containing 2 mM $CaCl_2$, (buffer A), post-fixed in 1.5 % potassium ferrocyanide and 2% osmium tetroxide (OsO_4) in buffer A for ~6 hrs at room temperature (RT). The tissues were then rinsed in buffer A, treated with 0.1% aqueous thiocarbohydrazide for 20 min at RT, rinsed again in distilled water, and was again treated with 2% OsO_4 for 30 min. The osmified specimens were washed in distilled water and subjected to en-block staining with 1% uranyl acetate for overnight at 4 °C, dehydrated in a graded series of ethanol solutions, and embedded in Durcupan ACM (Electron Microscopy Sciences, PA) in a vacuum oven, as described previously (9).

The tissue blocks were mounted on an aluminum pin, trimmed, and placed in a scanning electron microscope (FEI Quanta FEG) equipped with a block-face sectioning unit (Gatan Inc., 3 View system) as described (12). Backscatter electron images of the block-face were obtained, while material was removed from the flock-face at 70 nm increments using an oscillating diamond knife. Imaging was performed with a magnification of 8,000X and by a raster size of 4Kx4K pixels, using a 2.5kV accelerating voltage, spot size of 2.5, and pixel dwell time of 5 µsec. Similar to EM tomography, geometric features of membrane organelles were segmented in IMOD, triangular surface meshes were first generated in IMOD, refined in Biomedical Image-based Modeling and Simulation (BIMoS, www.bimos.org), and visualized in Amira.

References for Supporting Material: Methods

1. Zhou, Y. Y., S. Q. Wang, W. Z. Zhu, A. Chruscinski, B. K. Kobilka, B. Ziman, S. Wang, E. G. Lakatta, H. Cheng, and R. P. Xiao. 2000. Culture and adenoviral infection of adult mouse cardiac myocytes: methods for cellular genetic physiology. American journal of physiology. Heart and circulatory physiology 279:H429-436.
2. Soeller, C., D. Crossman, R. Gilbert, and M. B. Cannell. 2007. Analysis of ryanodine receptor clusters in rat and human cardiac myocytes. Proceedings of the National Academy of Sciences of the United States of America 104:14958-14963.

3. Jayasinghe, I. D., D. Baddeley, C. H. Kong, X. H. Wehrens, M. B. Cannell, and C. Soeller. 2012. Nanoscale Organization of Junctophilin-2 and Ryanodine Receptors within Peripheral Couplings of Rat Ventricular Cardiomyocytes. Biophysical journal 102:L19-21.
4. Baddeley, D., D. Crossman, S. Rossberger, J. E. Cheyne, J. M. Montgomery, I. D. Jayasinghe, C. Cremer, M. B. Cannell, and C. Soeller. 2011. 4D Super-Resolution Microscopy with Conventional Fluorophores and Single Wavelength Excitation in Optically Thick Cells and Tissues. PLoS One 6:e20645.
5. Tokunaga, M., N. Imamoto, and K. Sakata-Sogawa. 2008. Highly inclined thin illumination enables clear single-molecule imaging in cells. Nature methods 5:159-161.
6. Baddeley, D., M. B. Cannell, and C. Soeller. 2010. Visualization of localization microscopy data. Microsc Microanal 16:64-72.
7. Manders, E. M. M., F. J. Verbeek, and J. A. Aten. 1993. Measurement of co-localization of objects in dual-colour confocal images. Journal of Microscopy 169:375-382.
8. Jayasinghe, I. D., M. B. Cannell, and C. Soeller. 2009. Organization of ryanodine receptors, transverse tubules, and sodium-calcium exchanger in rat myocytes. Biophysical Journal 97:2664-2673.
9. Hayashi, T., M. E. Martone, Z. Yu, A. Thor, M. Doi, M. J. Holst, M. H. Ellisman, and M. Hoshijima. 2009. Three-dimensional electron microscopy reveals new details of membrane systems for Ca2+ signaling in the heart. Journal of cell science 122:1005-1013.
10. Lawrence, A., J. C. Bouwer, G. Perkins, and M. H. Ellisman. 2006. Transform-based backprojection for volume reconstruction of large format electron microscope tilt series. Journal of structural biology 154:144-167.
11. Kremer, J. R., D. N. Mastronarde, and J. R. McIntosh. 1996. Computer visualization of three-dimensional image data using IMOD. Journal of structural biology 116:71-76.
12. West, J. B., Z. Fu, T. J. Deerinck, M. R. Mackey, J. T. Obayashi, and M. H. Ellisman. 2010. Structure-function studies of blood and air capillaries in chicken lung using 3D electron microscopy. Respir Physiol Neurobiol 170:202-209.

Supplementary Figures

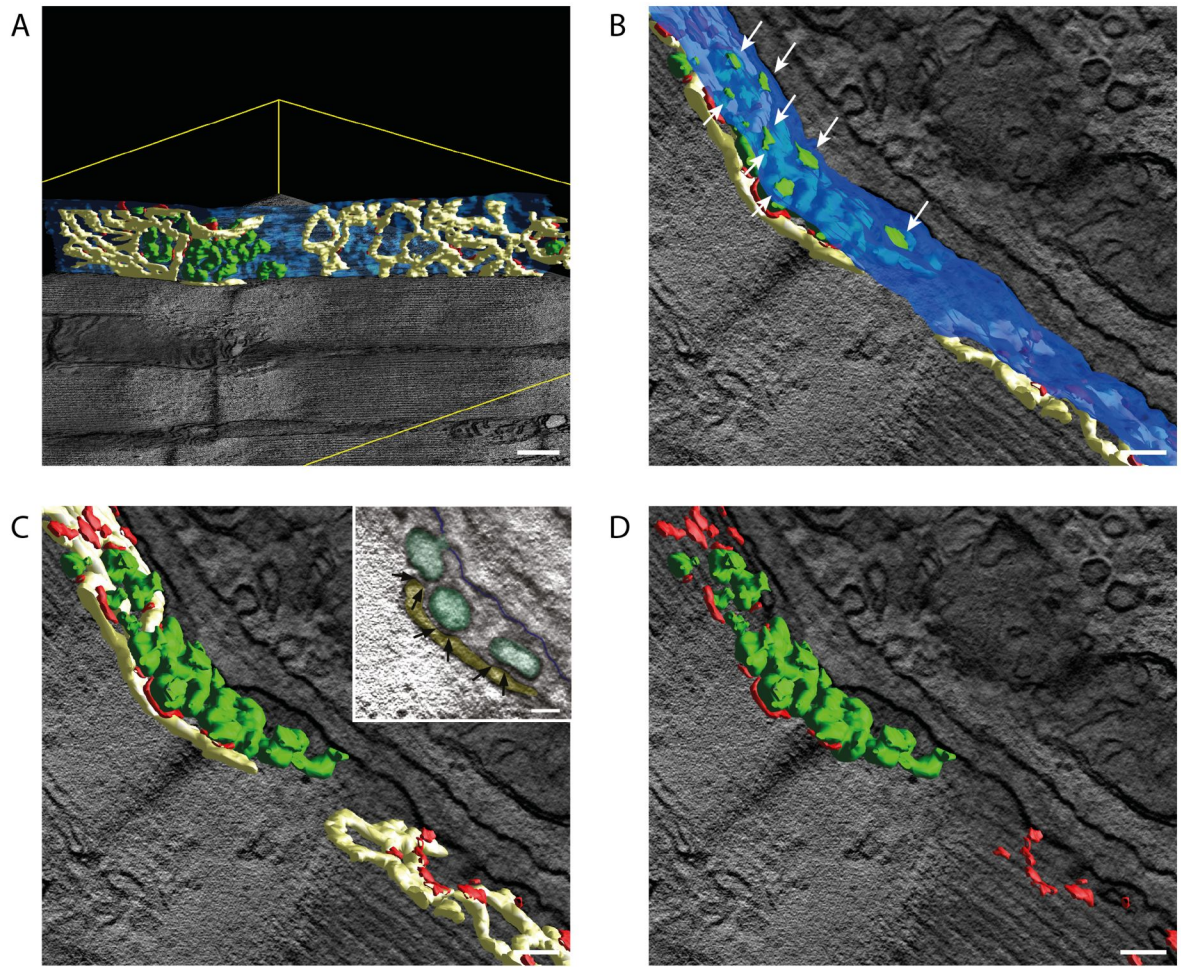

Fig. S1. Additional views of caveolae and sub-sarcolemmal SR at the surface sarcolemma. The figure shows several views of sarcolemma (blue), surface caveolae (green), couplings (red) and sub-sarcolemmal SR (pale yellow). **A**. View of the sarcolemma from the cytoplasmic side. Panels **B-D** look onto the sarcolemma slightly from the extra-cellular side. Caveolae openings are visible in green in B (see arrows). The inset in C shows a "thin section micrograph" extracted as a slice from the tomogram in which electron-dense "feet" are visible spanning the gap between caveolar (green) and peripheral SR (pale yellow) membranes, see arrows. The anatomical features were segmented from the EM tomogram data set also shown in Fig. 1 C&D, main text. Scale bars, A 200 nm; B-D 100 nm; C inset 50nm.

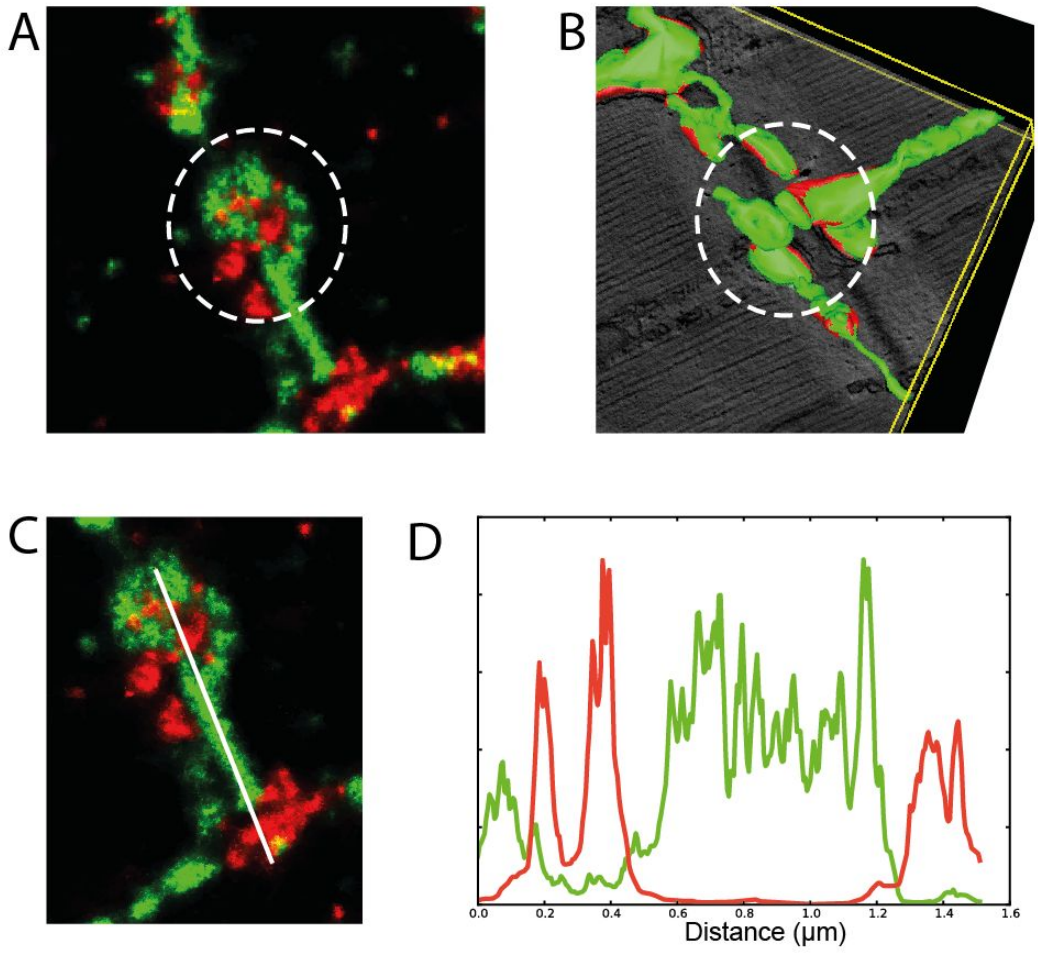

Fig. S2. Detail views of junctional t-system regions. The comparison of a super-resolution micrograph of a junctional area (**A**), in which CAV3 (green) and RyR (red) labelling are shown, with a segmented tomogram (**B**) that shows t-system membrane (green) and junctions (red) shows remarkable qualitative similarity in the main morphology. Note the local enlargement of t-system lumen where junctions are clustered in B. The good qualitative correlation suggests that CAV3 acts effectively as a tracer for t-system (outside of junctions, see **C & D**). In addition, it suggests that RyR labelling in the circled area in A is associated with junctions between t-system and SR. **C**. A profile through a region with strong RyR (red) labelling shows that CAV3 expression (green) is strongly anti-correlated with RyR expression (**D**) and we conclude that CAV3 expression is greatly reduced in t-system membrane sub-domains which contribute to junctions.

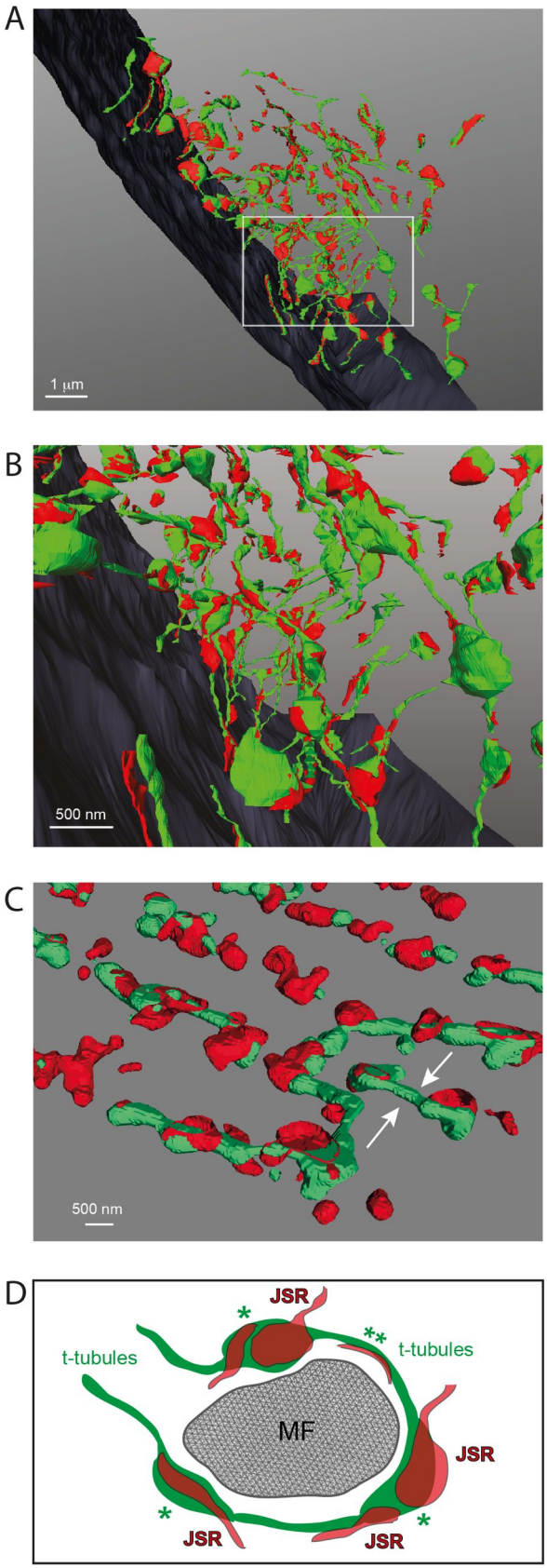

Fig. S3. Additional views of SBF-SEM data and iso-surface rendered 3D super-resolution data set. **A, B**, rendered SBFSEM segmentation. B is a high magnification view of the area indicated in A. T-system (green) branches originate from the sarcolemma (indigo blue) and constitute a lattice meshwork in the cytoplasm of a ventricular cardiomyocytes. Significant variation in the thickness of T-system branches is observed. In particular ampullae are found where junctions (red) are associated with the T-system membrane. **C**. Rendered 3D super-resolution data set of CAV3 (green) and RyR (red) recorded in a stained mouse cardiac myocyte. Note the relatively narrow t-tubule segments (traced by CAV3 signal, e.g. arrows) connecting regions with positive RyR labelling that exhibit increased luminal volume. **D**. A simplified schematic that summarizes the architecture of the t-tubules in the vicinity of a myofibril (MF) in cross-section as revealed by our data. The t-tubules (green) tend to exhibit local distensions in regions where the junctional SR (JSR, red) apposes t-tubules (areas marked by *) although some junctions are also in areas that show no particular change in diameter (**). Note that the schematic includes parts of the network SR (also in red) that connect the JSR sacs to the remainder of the SR.

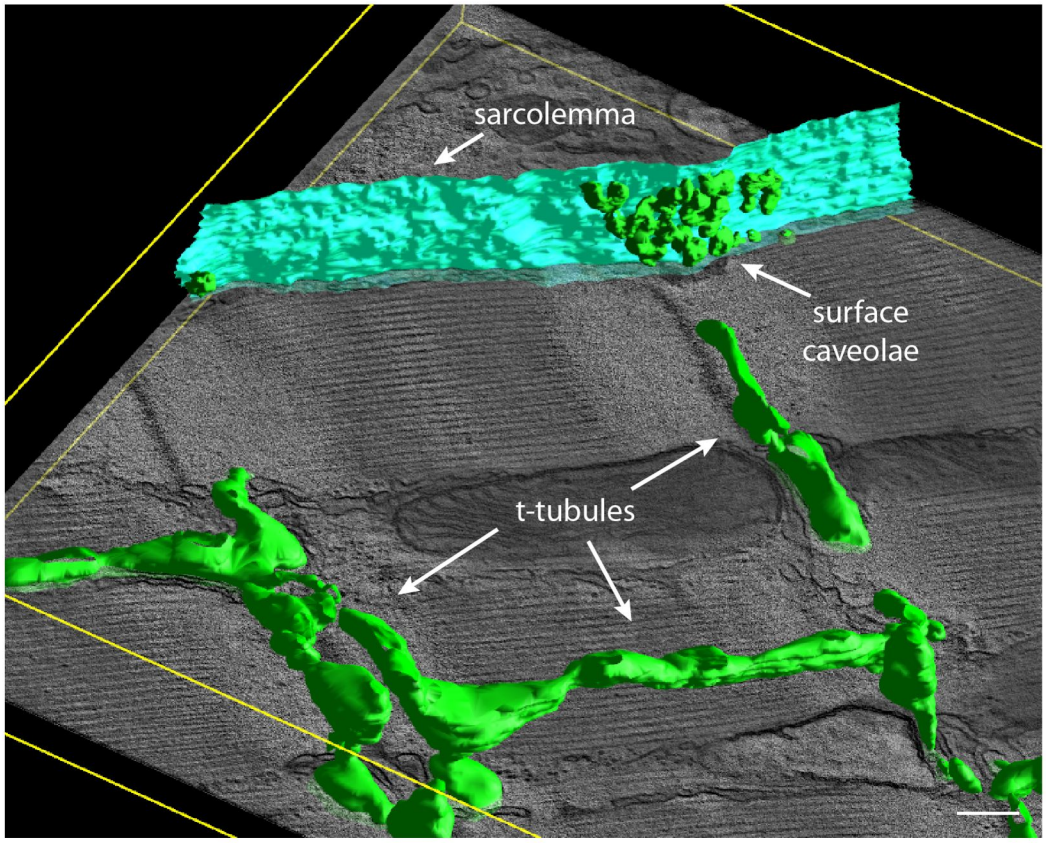

Fig. S4. Comparison of surface caveolae appearance to t-tubule membrane morphology. T-system segmentation was added to the tomogram data set shown in Fig. 1 C&D and Fig. S1. On qualitative inspection the t-tubule membranes show no obvious signs of extensive caveolae-like "mushroom-shaped" protrusions that would match the size and shape of the surface caveolae. Scale bar, 200 nm.

Supplementary Videos

Video S1. This movie shows several views of the 3D rendered segmentation of a region near the surface sarcolemma (blue). Surface caveolae (green), couplings (red) and sub-sarcolemmal SR (pale yellow) were segmented from the tomogram data as shown in Fig. S1.

Video S2. A movie showing a fly-through the segmented t-system and JSR obtained from the SBF-SEM data. Additional still views of these structures are shown in Fig. 3 and Fig. S3. The colour coding is t-system - green, surface sarcolemma - indigo blue and junctional SR membranes - red.

	% of RyR co-localizing with CAV3	% of CAV3 co-localizing with RyR	n (cells)	n (animals)
Surface sarcolemma	4.8 ± 0.7	3.5 ± 0.9	6	3
t-system/interior junctions	9.2 ± 1.2	9.0 ± 1.2	6	3

Table S1: Summary of percentages of co-localization between RyR and CAV3 from super-resolution microscopy data (Mean ± SEM).